COLELLA, R. (1974). *Acta Cryst.* A**30**, 413-423.
EWALD, P. P. & HENO, Y. (1968). *Acta Cryst.* A**24**, 5-15.
HART, M. & LANG, A. R. (1961). *Phys. Rev. Lett.* **7**, 120-121.
HØIER, R. & AANESTAD, A. (1981). *Acta Cryst.* A**37**, 787-794.
HØIER, R. & MARTHINSEN, K. (1983). *Acta Cryst.* A**39**, 854-860.
HÜMMER, K. & BILLY, H. W. (1982). *Acta Cryst.* A**38**, 841-848.
HÜMMER, K. & BILLY, H. W. (1986). *Acta Cryst.* A**42**, 127-133.
HÜMMER, K., WECKERT, E. & BONDZA, H. (1989). *Acta Cryst.* A**45**, 182-187.
JAGODZINSKI, H. (1980). *Acta Cryst.* A**36**, 104-116.
JURETSCHKE, H. J. (1982*a*). *Phys. Rev. Lett.* **48**, 1487-1489.
JURETSCHKE, H. J. (1982*b*). *Phys. Lett.* **92A**, 183-185.
LADD, M. F. C. & PALMER, R. A. (1980). Editors. *Theory and Practice of Direct Methods in Crystallography*, p. 23. New York: Plenum Press.
LIPSCOMB, W. N. (1949). *Acta Cryst.* **2**, 193-194.
MO, F., HAUBACH, B. C. & THORKILDSEN, G. (1988). *Acta Chem. Scand. Ser. A*, **42**, 130-138.
POST, B. (1977). *Phys. Rev. Lett.* **39**, 760-763.
POST, B., NICOLOSI, J. & LADELL, J. (1984). *Acta Cryst.* A**40**, 684-688.
SHEN, Q. (1986). *Acta Cryst.* A**42**, 525-533.
SHEN, Q. & COLELLA, R. (1988). *Acta Cryst.* A**44**, 17-21.
TANG, M. T. & CHANG, S. L. (1988). *Acta Cryst.* A**44**, 1073-1078.
THORKILDSEN, G. (1987). *Acta Cryst.* A**43**, 361-369.

Acta Cryst. (1989). A**45**, 708-715

The Pulsed-Neutron Diffraction Method of Studying Acoustic Phonons in Barium Fluoride and Calcium Fluoride

BY C. J. CARLILE

*Rutherford Appleton Laboratory, Chilton, Didcot, Oxon OX*11 0*QX, England*

AND B. T. M. WILLIS

Chemical Crystallography Laboratory, 9 *Parks Road, Oxford OX*1 3*PD, England*

(*Received* 22 *March* 1989; *accepted* 17 *May* 1989)

Abstract

Earlier papers [Willis (1986). *Acta Cryst.* A**42**, 514-525; Schofield & Willis (1987). *Acta Cryst.* A**43**, 803-809] have discussed the nature of the thermal diffuse scattering (TDS) arising from the interaction of a 'white' beam of thermal neutrons with the acoustic modes of vibration in a single crystal. A simpler version of the scattering theory is now given which does not have recourse to the numerous equations employed in previous treatments. The theory is applied to the interpretation of TDS data from BaF_2 and CaF_2 to give the velocity of sound in these crystals as a function of the direction of propagation.

1. Introduction

This paper is concerned with the scattering of pulsed neutrons, where each pulse contains a wide band of neutron wavelengths, by acoustic phonons in a single crystal. The theoretical treatment for *monochromatic* neutrons, scattered by phonons through a *variable* angle, has been covered by Seeger & Teller (1942), Waller & Froman (1952) and Lowde (1954). The pulsed neutron case, dealing with a *white* beam of neutrons scattered at a *fixed* angle, has unusual features which do not occur in the monochromatic case. These features give rise to the possibility of carrying out novel inelastic experiments, as we shall describe later.

The main features of the scattering theory for pulsed neutrons have been described by Willis (1986) and by Schofield & Willis (1987). For slower-than-sound neutrons, scattered at a fixed angle close to 180° (*i.e.* in back scattering), there is a wavelength window in the incident beam for which thermal diffuse scattering is forbidden. One edge of the window is associated with the absorption of acoustic phonons, and the other edge with their emission. By measuring the cut-off wavelengths for different angles of offset from the Bragg position, it is possible to determine the velocity of these acoustic phonons as a function of their direction of propagation. Earlier results from pyrolytic graphite have been given by Willis, Carlile, Ward, David & Johnson (1986).

In the next section we show how the principal results of the scattering theory can be derived using simple geometrical arguments alone. It is assumed that the crystal is elastically isotropic, whereas all crystals (including cubic crystals) are elastically anisotropic. For this reason the analysis is extended in §3 to the anisotropic case. Experimental results on the isomorphous crystals barium fluoride and calcium fluoride, which have different degrees of elastic anisotropy, are presented in § 4.

0108-7673/89/100708-08$03.00

2. Properties of the scattering surface

For both elastic and inelastic scattering processes, we define the scattering surface as the locus in reciprocal space of the end-point of the wave vector, **k**, of the scattered radiation. (**k** is a vector which lies along the scattering direction and has a magnitude of 2π/scattered wavelength.) In a fixed-wavelength variable-angle experiment the scattering surface is derived by plotting the end-point of **k** for different values of the scattering angle 2θ; for a white-beam fixed-angle experiment it is obtained by plotting the end-point of **k** for different values of the incident wavelength. For these two experimental arrangements the scattering surfaces are quite different, both for elastic and for inelastic processes. Thus there are four cases which we shall discuss separately in the following sections.

(i) *Elastic scattering*

(*a*) *Fixed wavelength.* Fig. 1 shows the reciprocal lattice with its origin at *O*. $\mathbf{k}_0$ is the wave vector of the incident neutrons and 2θ, the scattering angle, is the angle between $\mathbf{k}_0$ and **k**. The incident wavelength, λ, is fixed and so the magnitude of $\mathbf{k}_0$ $(=2\pi/\lambda)$ is also fixed. For elastic scattering, there is no exchange of energy with the crystal, and consequently k is equal to k_0. The point Q in Fig. 1 is the end-point of **k** and, as 2θ varies, Q moves along the surface of a sphere: the Ewald sphere. If the sphere passes through a reciprocal-lattice point, then Bragg scattering takes place from that point. Provided there is no kind of disorder in the crystal (for example, chemical, isotopic, magnetic, ...) this is the only elastic scattering process possible.

(*b*) *Fixed angle.* Next we consider a pulsed-neutron experiment in which a white beam containing a wide range of wavelengths strikes a stationary crystal. The scattered neutrons are observed at a single fixed angle 2θ.

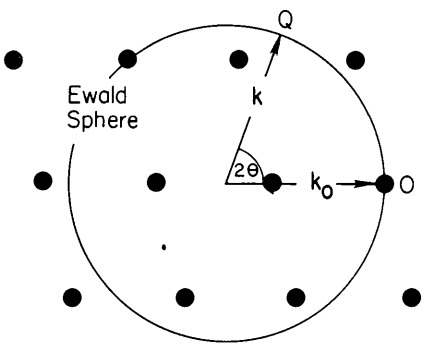

Fig. 1. The scattering surface for elastic scattering of monochromatic neutrons at a variable scattering angle 2θ. k_0 is inversely proportional to the neutron wavelength.

Fig. 2 is the diagram in reciprocal space corresponding to Fig. 1. $\mathbf{k}_0$ terminates at the origin *O*. Its length (k_0) varies inversely with the incident wavelength, but, for a given value of k_0, the wave number k of the scattered radiation is also equal to k_0. Clearly, the elastic scattering surface is the straight line *OR* in Fig. 2, which is inclined at an angle of $\pi/2-\theta$ to the incident beam. In three dimensions the scattering surface is therefore a right-circular cone with its axis along $\mathbf{k}_0$ and with a semi-angle of $\pi/2-\theta$. Bragg scattering can only occur if θ is chosen so that the cone passes through a reciprocal-lattice point.

Both scattering surfaces in (i) (*a*) and (i) (*b*) were first discussed by Ewald (1919). In the fixed-wavelength case the surface is known as the Ewald sphere; in the fixed-angle case we shall refer to the surface as 'the Ewald cone'.

(ii) *Inelastic scattering*

(*a*) *Fixed wavelength.* We shall now consider one-phonon inelastic scattering in which the scattered neutron exchanges a quantum of vibrational energy with the crystal. The topology of the inelastic scattering surface is governed by the conservation relations for energy and momentum.

For scattering by long-wavelength acoustic modes of vibration (*i.e.* sound waves), energy conservation requires that (Willis, 1986)

$$k-k_0=-\varepsilon\beta q, \tag{1}$$

where q is the wave number of the sound wave, assumed small, and β is the ratio of the phase velocity of sound in the crystal to the incident neutron velocity:

$$\beta=c_s/v_n. \tag{2}$$

ε in (1) can be either $+1$ or -1: $+1$ refers to phonon creation and neutron energy loss, and -1 to phonon annihilation and neutron energy gain.

Momentum conservation requires that the phonon wave vector **q** is the vector joining the end-point of **k** with the nearest point of the reciprocal lattice.

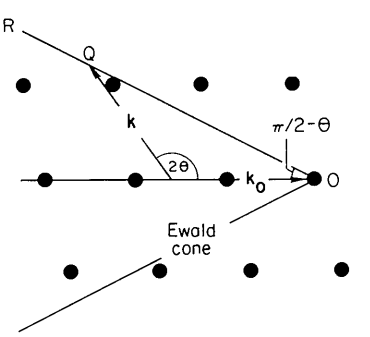

Fig. 2. The scattering surface for elastic scattering of 'white' neutrons at a fixed scattering angle 2θ.

In the neighbourhood of the reciprocal-lattice point P, we have the situation shown in Fig. 3(a). When Q, the end-point of $\mathbf{k}$, lies inside the Ewald sphere, $k < k_0$ and scattering occurs by energy loss. Since the wave number of sound waves is much less than that of thermal neutrons, *i.e.* $q \ll k_0$, the Ewald sphere can be replaced to a good approximation by its tangential plane normal to the scattered direction, as shown on an enlarged scale in Fig. 3(b). In scanning across the reciprocal-lattice point by varying 2θ, the representative point Q traces out the locus shown as $QQ'Q''\ldots$ in Fig. 3(b). The perpendicular distance of Q from the Ewald surface is $k_0 - k$, which is equal to βq from (1) with $\varepsilon = +1$. q is the distance of Q from the fixed point P. Hence the ratio QP/QN is $1/\beta$, and, provided that the velocity of sound in the crystal is independent of its direction of propagation, the locus of Q is a conic with eccentricity $1/\beta$. If the neutron velocity exceeds the sound velocity ($\beta < 1$), the inelastic-scattering surface is a rotational hyperboloid, whereas if the neutrons are slower than the sound velocity ($\beta > 1$), the scattering surface is a rotational ellipsoid.

These surfaces are illustrated in Fig. 4(a) for faster-than-sound neutrons and in Fig. 4(b) for slower-than-sound neutrons. Two sets of surfaces are drawn, each set corresponding to a different distance of the reciprocal-lattice points P_1 and P_2 from the Ewald sphere. The contribution of thermal diffuse scattering to the measured Bragg intensity is derived by summing the individual contributions of those phonon states in Fig. 4 which lie on the scattering surfaces and can be seen by the detector. The resultant scattering patterns are illustrated in Fig. 5. For faster-than-sound neutrons, the TDS rises to a maximum at the centre of the Bragg peak because the number of states contributing to the TDS remains unchanged during the scan, while the intensity per phonon state varies as $1/q^2$. On the other hand, for slower-than-sound neutrons the TDS is constant across the Bragg peak, because the increase in intensity arising from the $1/q^2$ term is exactly balanced by a progressive reduction in the number of accessible states as the centre of the peak is approached (Willis, 1970).

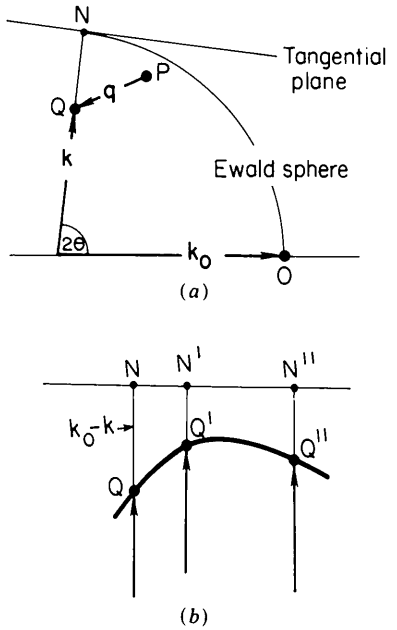

Fig. 3. (a) The inelastic scattering of monochromatic neutrons in the case of neutron energy loss ($\varepsilon = +1$). The process is shown on an enlarged scale in (b).

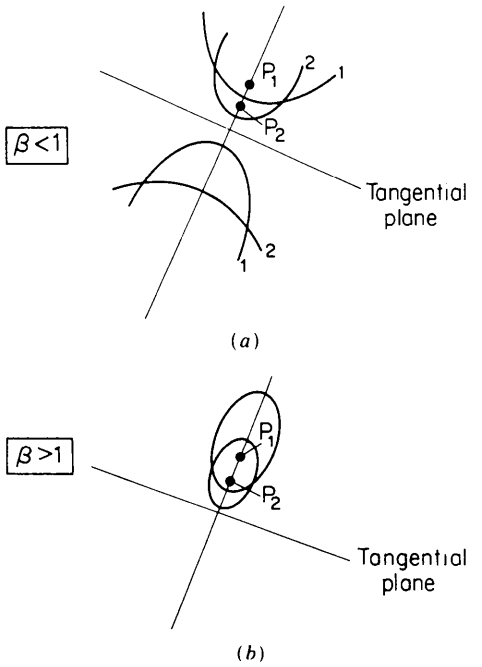

Fig. 4. Inelastic scattering surfaces for monochromatic neutrons scattered through a variable angle 2θ. (a) Incident neutrons faster than sound, permitting both energy loss and energy gain. The surfaces are hyperboloidal. (b) Incident neutrons slower than sound, where only energy gain is possible. The surfaces are ellipsoidal.

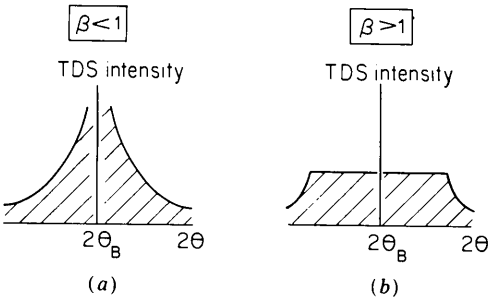

Fig. 5. The TDS intensity in the neighbourhood of a Bragg peak, scanned as a function of scattering angle 2θ at constant neutron wavelength: (a) faster-than-sound neutrons; (b) slower-than-sound neutrons.

(*b*) *Fixed angle.* The derivation of the topology of the scattering surface follows exactly the same procedure as in (ii) (*a*), apart from one important difference. The scattering surface is now inclined at an angle of $\pi/2-\theta$ to the scattering direction, whereas in (ii) (*a*) these two directions are perpendicular to one another. Thus Fig. 3 must be redrawn as Fig. 6.

The perpendicular distance QN of Q in Fig. 6(*a*) from the Ewald cone is $(k_0-k)\cos\theta=\beta q\cos\theta$, and so the ratio QP/QN is $1/(\beta\cos\theta)$. As in the fixed-wavelength case, the inelastic scattering surface is a conic, but its eccentricity is $(\sec\theta)/\beta$, rather than $1/\beta$. This is shown on an enlarged scale in Fig. 6(*b*). In scanning across the reciprocal-lattice point by varying the incident wavelength λ the representative point Q traces out the locus shown as $QQ'Q''$. The properties of the surface are described conveniently under the three ranges of β: (1) $\beta<1$, (2) $1<\beta<\sec\theta$, (3) $\beta>\sec\theta$. We shall ignore case (3) because, since θ is almost equal to $\pi/2$ for the measurements to be described later, $\sec\theta$ tends to infinity and case (3) is not encountered. There remain two categories, $\beta<1$ and $\beta>1$, and for *both* these the scattering surface is a rotational hyperboloid. Only for the third case of $\beta>\sec\theta$ is the scattering surface an ellipsoid.

However, there is a fundamental distinction between the scattering surfaces for faster-than-sound neutrons ($\beta<1$) and for slower-than-sound neutrons ($\beta>1$). This is illustrated by Fig. 7, which is drawn to scale for a scattering angle of 170° and for $\beta=1{\cdot}2$. There is a finite band of wavelengths for which neither branch of the scattering surface is intersected by the scattered wave vector: hence, for slower-than-sound neutrons one-phonon scattering is forbidden within a certain wavelength range, or window, of the incident radiation. There is no such window for faster-than-sound neutrons, because the scattered wave vector **k** intersects both branches of the scattering surface at all incident wavelengths.

The width of the wavelength window $\Delta\lambda$ is proportional to the Bragg offset angle $\Delta\theta$, which is defined as the angle in the scattering plane required to bring the crystal to the Bragg reflecting position. From equation (40) of Willis (1986) the total width of the window for back scattering with $2\theta\rightarrow 2\theta_B=\pi$ is

$$\Delta\lambda=\lambda_B(\beta^2-1)^{1/2}\,\Delta\theta \qquad (3)$$

where λ_B is the wavelength for Bragg scattering. The cut-off wavelengths are

$$\lambda_B\pm(1/2)\,\Delta\lambda$$

and so, if the offset angle is small, the wavelengths at the two edges of the window are symmetrically located on either side of the Bragg wavelength.

The form of the TDS in scanning through the Bragg peak in a fixed-angle experiment is illustrated in Fig. 8. The faster-than-sound case in Fig. 8(*a*) is very similar to that in Fig. 5(*a*) for a constant-wavelength scan, whereas the slower-than-sound case in Fig. 8(*b*) bears no resemblance to Fig. 5(*b*).

The appearance of the edges indicated in Fig. 8(*b*) enables novel experiments to be carried out by the pulsed neutron method. The wavelengths of the edges are readily measured by time of flight, and then (3) is used to determine β from the slope at the cross-over point of $\Delta\lambda$ *versus* $\Delta\theta$. Taking the neutron velocity v_n as that of the neighbouring Bragg peak, the sound velocity is given by (2). The direction of propagation with respect to the normal to the Bragg

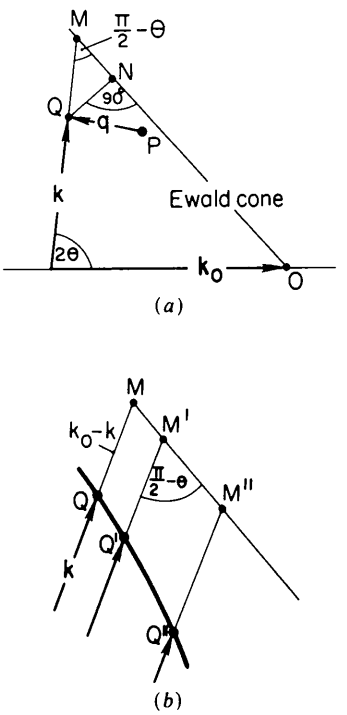

Fig. 6. (*a*) The inelastic scattering of 'white' neutrons in the case of neutron-energy loss ($\varepsilon=+1$). The process is shown on an enlarged scale in (*b*). The scattering angle is variable in Fig. 3 but is fixed in Fig. 6.

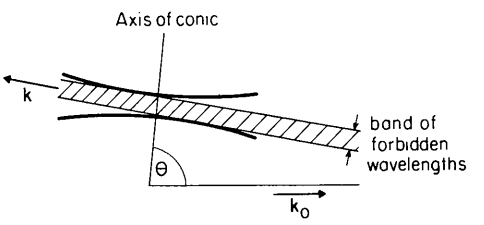

Fig. 7. The inelastic scattering surfaces for 'white' neutrons scattered through a fixed angle 2θ. θ_B has been chosen to be 90° and 2θ to be 170°. There is a finite band of incident wavelengths in the neighbourhood of the Bragg wavelength for which an intersection is not possible between **k** and the scattering surfaces.

plane is derived using the expression

$$\zeta = \pi/2 \pm \arcsin(1/\beta)$$

[see equation (41) of Willis (1986)].

3. Elastically anisotropic crystals

We now consider the question of elastic anisotropy. It has been assumed so far that β is constant: this assumption is not valid for the vast majority of crystals, which are elastically anisotropic and propagate sound at a velocity varying with direction.

The scattering surfaces in § 2 were drawn for the scattered wave vector **k** extending throughout the whole of reciprocal space. However, the location of the edge of the wavelength window is determined by the single point in reciprocal space where **k** is tangential to the scattering surface; we shall now show that, for either the isotropic or the anisotropic propagation of sound, this point can be located without considering the topology of the rest of the scattering surface. (We have shown that the scattering surface is described by a simple conic for isotropic propagation; the surface is considerably more complex for anisotropic propagation.)

Fig. 9 shows an arbitrary vector **k** terminating at a point Q on the scattering surface. The energy of the neutron at Q is

$$E_n = \hbar^2 k^2 / 2m_n$$

with $\hbar = h/2\pi$ and m_n the neutron mass. If Q is shifted along the scattering surface to Q' by an incremental amount $dk = QQ'$ then the incremental change of energy is

$$dE_n = (\hbar^2 k/m_n)\, dk = \hbar v_n\, dk. \qquad (4)$$

The condition for **k** to be a tangent to the scattering surface is that the line QQ' is collinear with the scattered direction, as illustrated in Fig. 9.

The change in the neutron energy dE_n is exactly counterbalanced by a corresponding change in the vibrational energy of the crystal. The phonon associated with Q is **q**, which is the vector to the reciprocal-lattice point P, and the phonon associated with Q' is **q**′ (see Fig. 9). The energy of the phonon **q** is

$$E_{ph} = \hbar\omega(\mathbf{q})$$

where $\omega(\mathbf{q})$ is its (circular) frequency. Thus the incremental change in phonon energy between Q and Q' is the scalar product

$$dE_{ph} = \mathrm{grad}_{\mathbf{q}}[\hbar\omega(\mathbf{q})].\hat{\mathbf{k}}\, dk \qquad (5)$$

with $\hat{\mathbf{k}}$ denoting a unit vector.

The conservation of energy requires that

$$dE_{ph} = -dE_n$$

for scattering by neutron-energy loss ($\varepsilon = +1$), and

$$dE_{ph} = +dE_n$$

for scattering by neutron-energy gain ($\varepsilon = -1$). From (4) and (5) we obtain the expression

$$v_n = \varepsilon\, \mathrm{grad}_{\mathbf{q}}[\omega(\mathbf{q})].\hat{\mathbf{k}}. \qquad (6)$$

Equation (6) has a very simple interpretation. $\mathrm{grad}_{\mathbf{q}}[\omega(\mathbf{q})]$ denotes the group velocity of sound in the crystal, and so the edge of the wavelength window corresponds to that neutron velocity in the incident beam which is equal to the group velocity resolved in the direction of the scattered beam. Moreover, the TDS intensity rises to a sharp maximum at the edge, because the density of phonon states which contribute to the intensity for a fixed $\mathbf{k}_0$ increases sharply as **k** touches the scattering surface.

For isotropic sound propagation, the group velocity and phase velocity are the same. All the formulae derived by Willis (1986) for isotropic propagation can be used for anisotropic propagation, provided that β is replaced by β_g. β is defined as the ratio of the phase velocity to the incident neutron velocity, whereas β_g is the ratio of the group velocity to the incident neutron velocity.

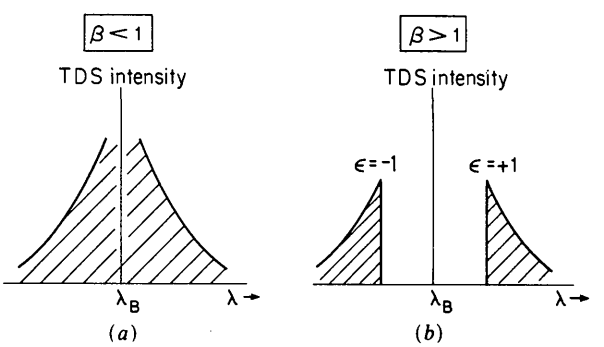

Fig. 8. The form of the TDS intensity in scanning through the Bragg peak with 'white' neutrons at a constant angle: (*a*) faster-than-sound; (*b*) slower-than-sound neutrons.

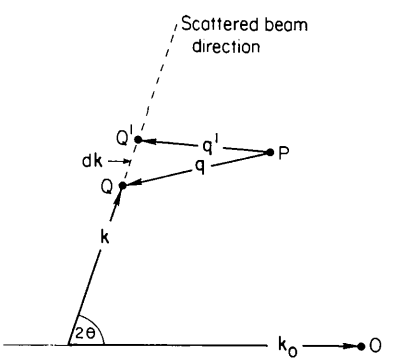

Fig. 9. 'White' neutrons scattered through a fixed angle with energy gain. The condition that **k** is a tangent to the scattering surface is that QQ' lies along the direction of the scattered beam.

4. Experimental measurements

The elastic constants of a crystal are represented by a fourth-rank tensor, so that cubic, as well as non-cubic, crystals are elastically anisotropic. However, under certain special circumstances cubic crystals are nearly isotropic. Cubic crystals possess three elastic stiffness constants, c_{11}, c_{12}, c_{44}, and if these constants satisfy the Cauchy relation

$$c_{11} - c_{12} = 2c_{44}, \tag{7}$$

sound waves are propagated with the same velocity in all directions. The Cauchy relation is obeyed approximately by barium fluoride at room temperature, because the anisotropy factor $[(c_{11} - c_{12})/2c_{44}]$ of 0·97 (Gerlich, 1964) is close to unity. On the other hand, the anisotropy factor of the isomorphous calcium fluoride is 1·64 and so this crystal is distinctly anisotropic.

The experimental measurements were carried out on the High Resolution Powder Diffractometer (HRPD) at the ISIS Pulsed Neutron Source (Johnson & David, 1985). Fig. 10 shows the TDS pattern in the vicinity of the 422 reflection from BaF_2 and for 20 detectors, each observing a different angle of offset. In the centre of each pattern there is the TDS window, which is bounded by edges with a steeply rising intensity. Theory indicates that the intensity should rise vertically, but this does not occur in practice because of the finite range of scattering angles, 2θ, which is covered by each detector element. For the 2 m position of the sample from the detector, this range is 0·4° in 2θ. $\Delta\theta$ in Fig. 10 is $(\theta_B - \theta)$, and so the TDS pattern recorded in each detector does not correspond to a sharply defined offset angle but to offset angles spread over a range of 0·2°.

The crystal was oriented to bring the 440 reflection into exact back scattering, *i.e.* $\theta_B = 90°$. Scattering patterns were observed for scattering angles ranging from 170 to 178° using 40 detectors grouped in two sets on either side of the incident beam. The positions in time of the edges of the TDS windows were determined from the individual patterns such as those shown in Fig. 10. These positions are plotted in Fig. 11 as a function of the scattering angle. The slope of the lines in Fig. 11 at a scattering angle 2θ of 180° is given by

$$R = \Delta t/(\Delta\theta t_B) = \Delta\lambda/(\Delta\theta\lambda_B)$$

where R is related to the sound velocity *via* (3). Note that the lines are not straight. Possible reasons for this are (i) a small departure from isotropy, (ii) phonon dispersion effects, and (iii) a breakdown in the theory for large offset angles.

A further point to note is the symmetry of the curves recorded in the detectors on either side of the Bragg reflection. This symmetry arises because the incident neutron beam lies in a vertical mirror plane of the crystal. Irregular features in the lines, which are reproduced on both sides of the detector bank (such as those indicated by *A* in Fig. 11), are real effects associated with the dynamical properties of the crystal. We are confident that this is not an instrumental effect since, as the crystal is moved from the

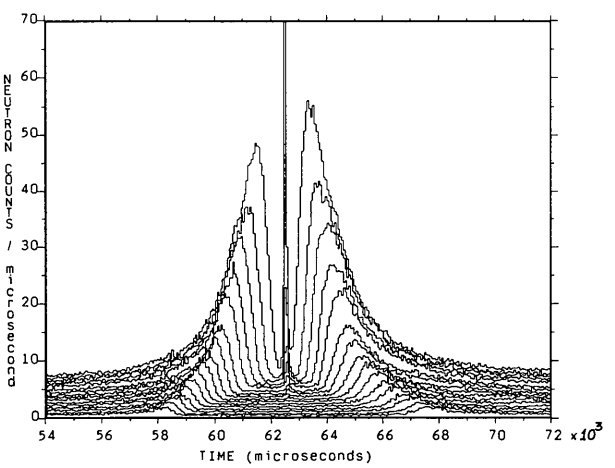

Fig. 10. The TDS pattern from the 422 reflection of barium fluoride. The phonon creation and phonon absorption peaks are clearly seen in each of the 20 detectors.

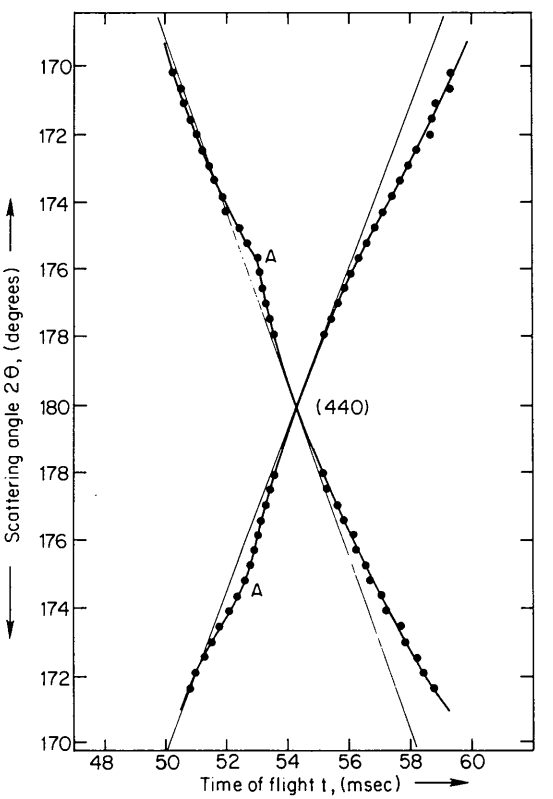

Fig. 11. The loci in time of flight of the phonon edges plotted *versus* offset angle $\Delta\theta$ for the 440 reflection from barium fluoride (observed in back scattering: $2\theta_B = 180°$).

Table 1. *Barium fluoride: calculated and observed sound velocities*

Reflection	Velocity calculated ($km\ s^{-1}$)	Velocity measured ($km\ s^{-1}$)	Direction of propagation
440	2·25	2·43	[100] 49° (110)
422	2·25	2·45	[100] 85° (110)

Table 2. *Calcium fluoride: calculated and observed sound velocities*

Reflection	Velocity calculated ($km\ s^{-1}$)	Velocity measured ($km\ s^{-1}$)	Direction of propagation
400	3·70	3·73	[100] 67° (110)
600	3·92	3·80	[100] 55° (110)

back-scattering condition, the irregular features follow the movement of the reflection.

Table 1 gives the sound velocities as determined from the wavelength windows associated with the 440 and 422 reflections from BaF_2. The agreement with the velocities calculated for the transverse modes from the elastic constants is good but not perfect: the neutron values are consistently about 10% higher than those calculated from the elastic constants. In the table the direction of propagation is given as the angle to the [100] direction and within the (110) plane.

Measurements were also made on a single crystal of calcium fluoride, which was oriented for the examination of $h00$ reflections in back scattering. The data are shown in Fig. 12 for one side of the detector bank. In the same manner as for BaF_2, the times of flight at the edges are plotted in Fig. 13 for the excitations associated with the 600 and 400 Bragg reflections. (Note that in the time-of-flight technique both reflections of the single crystal are observed simultaneously.) The velocities are derived from the slopes of the $\Delta\theta/\Delta t$ lines at $\Delta\theta = 0$ and are given in Table 2. They are within 3% of those calculated from the elastic constants.

The $\Delta\theta/\Delta t$ lines have a greater curvature for CaF_2 than for BaF_2. Thus the lines for both 400 and 600 in CaF_2 are skewed to longer times of flight for increasing offsets $\Delta\theta$, while the symmetry on either side of the Bragg position is retained. We believe that this difference between the two fluorides arises from the difference in their degrees of elastic anisotropy.

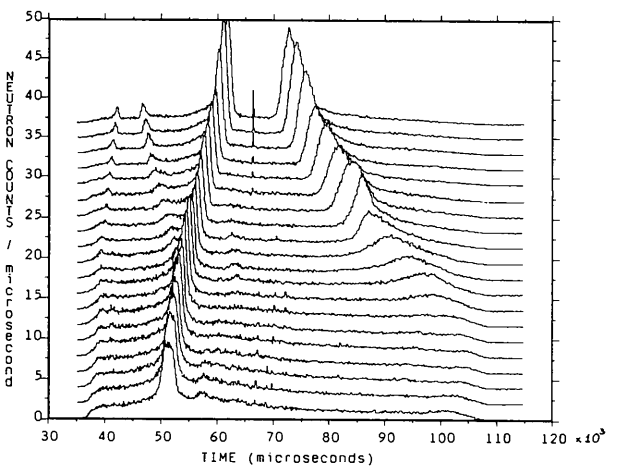

Fig. 12. The TDS pattern from the 400 and 600 reflections of calcium fluoride at $2\theta_B = 180°$.

Another significant feature is the repulsion of the $\Delta\theta/\Delta t$ lines which are associated with adjacent reflections, as indicated by B in Fig. 13. Similarly, the curvature at C is caused by a repulsion by excitations from the 200 reflection, which lies beyond our observational range.

5. Concluding remarks

We have shown that sound velocities can be measured in single crystals by means of a diffraction technique in which pulsed neutrons are employed without energy selection. Qualitative differences occur in the results from materials with different anisotropic factors. There appears to be no restriction on the type of crystal to be studied: for example optically opaque crystals can be examined, which are not accessible to measurement by Brillouin scattering.

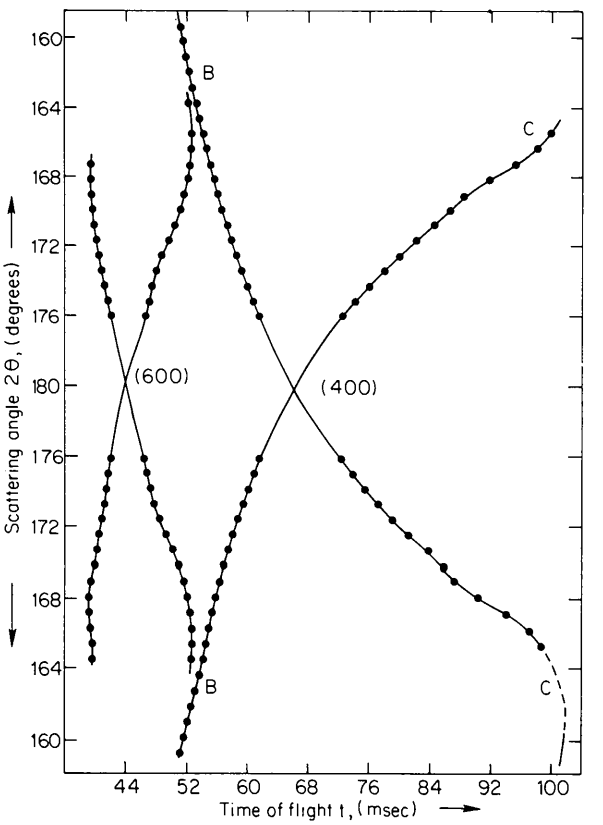

Fig. 13. The phonon edges derived from the data in Fig. 12 plotted in $\Delta\theta$, Δt space for the 400 and the 600 reflections of calcium fluoride.

We do not envisage that the present technique will be restricted to the determination of sound velocities. It can be used also to study the nature of acoustic vibrations in the vicinity of phase transitions, or to investigate excitations away from the origin of the Brillouin zone. These are the types of problem to be examined in future publications.

We thank Dr W. I. F. David and Mr R. M. Ibberson for their help in carrying out the neutron experiments on HRPD. We are also grateful to Professor A. Albinati for useful discussions.

References

EWALD, P. P. (1919). *Phys. Z.* **14**, 465-472.
GERLICH, D. (1964). *Phys. Rev.* **135**, A1331-A1333.
JOHNSON, M. W. & DAVID, W. I. F. (1985). Rep. RAL-85-112. Rutherford Appleton Laboratory, Didcot, Oxon, England.
LOWDE, R. D. (1954). *Proc. R. Soc. London Ser. A*, **221**, 206-223.
SCHOFIELD, P. & WILLIS, B. T. M. (1987). *Acta Cryst.* A**43**, 803-809.
SEEGER, R. J. & TELLER, E. (1942). *Phys. Rev.* **62**, 37-40.
WALLER, I. & FROMAN, P. O. (1952). *Ark. Fys.* **4**, 183-189.
WILLIS, B. T. M. (1970). *Acta Cryst.* A**26**, 396-401.
WILLIS, B. T. M. (1986). *Acta Cryst.* A**42**, 514-525.
WILLIS, B. T. M., CARLILE, C. J., WARD, R. C., DAVID, W. I. F. & JOHNSON, M. W. (1986). *Europhys. Lett.* **2**, 767-774.

Acta Cryst. (1989). A**45**, 715-718

The Use of *MULTAN* to Locate the Positions of Anomalous Scatterers

BY A. K. MUKHERJEE,* J. R. HELLIWELL†‡ AND P. MAIN

Department of Physics, University of York, Heslington, York YO1 5DD, England

(*Received* 2 *November* 1988; *accepted* 19 *May* 1989)

Abstract

Observed anomalous scattering differences have been used with the direct-methods program *MULTAN*87 to determine the positions of anomalous scatterers in a variety of metalloproteins and a small molecule. The lack of anomalous differences in the centric data did not prevent the determination of the atom positions and the anomalous scatterers were found in all cases. These results show that the method may be useful to determine the positions of anomalous scatterers in the case of multi-site genetically engineered proteins.

Introduction

Anomalous scattering measurements are increasingly being used in macromolecular crystal structure analysis because of the availability of synchrotron radiation. The variable wavelength makes available multiple-wavelength anomalous-dispersion data from which structures have now been determined by various groups. The technique can be readily applied to the metalloproteins. In addition, it is becoming easier to prepare heavy-atom derivatives and these need not be isomorphous with a native protein if multi-wavelength techniques are used.

The location of the metal atoms is required before phases can be calculated. A Patterson synthesis can be used with anomalous, isomorphous or combined differences, but the interpretation is straightforward when there are only a few sites. For more than about four sites, interpretation becomes less easy. However, with genetic engineering, the possibility of incorporating as many as 20 atoms into a molecule is not unreasonable.

Direct methods have been used to locate metal atoms in proteins on the basis of isomorphous differences [see, for example, Wilson (1978) and Adams, Helliwell & Bugg (1977)]. Given the prospect of a large number of metal sites and the possibility of using multi-wavelength methods, we decided to explore the use of anomalous differences with the direct-methods program *MULTAN*87 (Debaerdemaeker, Germain, Main, Tate & Woolfson, 1987) to locate the metal atoms. We have restricted ourselves to the use of the imaginary component ($\Delta f''$) derived differences, *i.e.* differences measured at one wavelength. These are inherently more accurate than the estimate of $\Delta f'$ from multiple-wavelength experiments because of difficulties with absorption corrections at the different wavelengths. The results are therefore applicable to both conventional and synchrotron X-ray sources.

Method

Anomalous differences can be expressed (Blundell & Johnson, 1976) as

$$\Delta_{\text{ano}} = |F^+| - |F^-| \simeq 2F''_{\text{ano}} \cos(\varphi - \varphi''_{\text{ano}}) = 2F''_{\text{ano}} \cos \Delta\varphi \quad (1)$$

where the symbols are defined in Fig. 1.

* Permanent address: Department of Physics, Jadavpur University, Calcutta-700032, India.
† Present address: Department of Chemistry, University of Manchester, Manchester M13 9PL.
‡ Author to whom correspondence should be addressed.

0108-7673/89/100715-04$03.00